Title
Comparison of Ureteral Stent Biomaterials: Encrustation Profile in Lithogenic Artificial Urine Models.

Journal
ACS Omega, 8(32)

Authors
Wu, Yi
Choi, Eric
Vu, Amberly
et al.

Publication Date
2023-08-15

DOI
10.1021/acsomega.3c01800

Peer reviewed

ACS OMEGA

http://pubs.acs.org/journal/acsodf

Article

Comparison of Ureteral Stent Biomaterials: Encrustation Profile in Lithogenic Artificial Urine Models

Yi X. Wu,* Eric J. Choi, Amberly A. Vu, Pengbo Jiang, Sohrab N. Ali, Roshan M. Patel, Jaime Landman, and Ralph V. Clayman

Cite This: *ACS Omega* 2023, 8, 29003−29011

Read Online

ACCESS | Metrics & More | Article Recommendations | Supporting Information

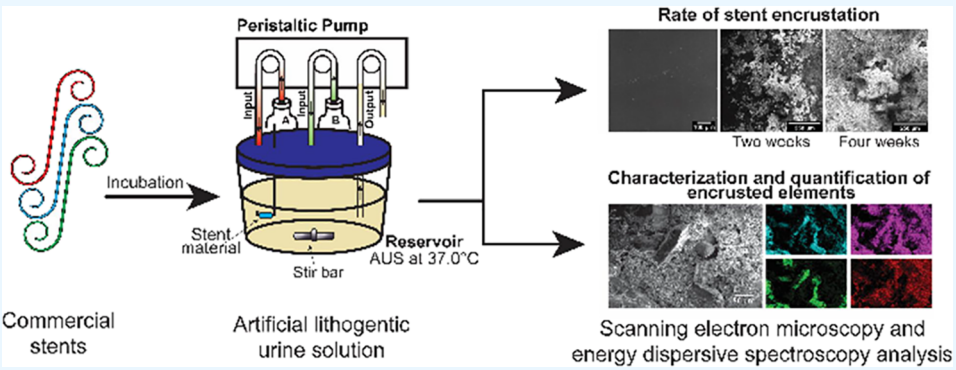

ABSTRACT: Ureteral stent encrustation significantly limits indwelling time and can lead to downstream urological problems. However, no ideal polymeric biomaterials have been shown to completely resist encrustation in long-term urine exposure. Recently, 2-hydroxyethyl methacrylate (HEMA)-coated Pellethane was reported as a promising biomaterial resistant to encrustation. This study compared HEMA-coated Pellethane to commercially available stents under two different artificial urine environments. To evaluate the degree and composition of encrustation on HEMA-coated Pellethane, Boston Scientific Tria, Bard InLay Optima, Cook Universa Hydrogel, and Cook Black Silicone stents were used at various dwelling times in two different artificial urine environments. In a batch−flow model, samples of stents were suspended in an artificial urine solution (AUS) at 37 °C. Every 24 h for 11 weeks, 50% of the AUS would be replaced with fresh components using a programmable peristaltic pump system. The stent materials were removed at suitable time intervals and air-dried for 24 h under sterile conditions before follow-up analysis. SEM was used to assess the degree of encrustation, and inductively coupled plasma mass spectrometry (ICP-MS) was employed to quantify the encrusted compositions, specifically for calcium, magnesium, and phosphorus. We measured the weight gain over time due to encrusted deposits on the stents and quantified the amount of Ca, Mg, and P deposited on each encrusted stent. After the 11 week trial, HEMA-coated Pellethane showed the most average mass change. SEM showed that HEMA-coated Pellethane was fully encrusted in just 2 weeks in the AUS environments, and ICP-MS showed that Ca is the most abundant deposit. Among all the tested stents, Black Silicone performed the best. The two AUSs were formulated to encrust more rapidly than physiological conditions. HEMA-coated Pellethane is not an ideal stent material, while silicone is a promising material for advancing ureteral stents.

1. INTRODUCTION

Since the introduction of allopathic devices 1976 to maintain patient ureters, ureteral stents have become the mainstay for decompressing obstruction and preventing occlusion after ureteroureterostomy, ureteral reimplantation, pyeloplasty, and endoscopic procedures.[1−3] A host of scenarios, such as ureteral trauma, tumors, iatrogenic injury, and infectious, obstructing renal stones, often require stent placement to relieve obstruction and preserve the kidney function.[4,5] Many of these conditions may require long-term decompression for chronic obstruction, for example, ureteral strictures or cancer with malignant obstructions.[6,7] Although stents are an indispensable tool of the urological arsenal, they have their setbacks. Unfortunately, these medical devices lose effectiveness over time as they frequently become obstructed by encrustation.[5,8] Despite improvements in biomaterials, encrustation remains a persistent impediment to urological care. Long-term indwelling ureteral stents often develop microbial biofilm and encrustations from urine exposure, leading to

Received: March 16, 2023
Accepted: July 20, 2023
Published: August 1, 2023

downstream ipsilateral ureteral obstruction and renal colic.[9] Furthermore, forgotten stents also result in undesirable financial burdens.[8,10,11]

A study by Cottone et al. recently demonstrated 2-hydroxyethyl methacrylate (HEMA)-coated Pellethane as a promising material for stents.[12] Pellethane is a family of biocompatible thermoplastic polyurethane (TPU) and has a long history in medical applications.[13] Their results suggested that HEMA-coated Pellethane was highly resistant to encrustation.[12]

In this study, we investigated and compared the encrustation formation in HEMA-coated Pellethane to that in commercially available polymer-based stents with various surface chemistries designed to resist the deposition of urinary elements leading to encrustation. For example, Universa Hydrogel contains AQ hydrophilic coating, Boston Scientific Tria uses Percushield technology, and Bard InLay maintains an ultra-smooth surface. Following previous in vitro batch−flow models, we evaluated the encrustation rates using two different artificial urine solutions (AUSs).[12,14] One of the AUSs replicated the formation of calcium oxalate (CaC_2O_4) stone, while the other simulated the environment to form infectious stones (struvite, $NH_4MgPO_4{\cdot}6H_2O$, and hydroxyapatite, $Ca_{10}(PO_4)_6(OH)_2$).

2. MATERIALS AND METHODS

2.1. Stents. This study compared five different stent materials to investigate their encrustation resistance in two different crystal-forming artificial urine environments. The stents of interest are Boston Scientific Tria (Boston Scientific Corporation, Marlborough, MA, USA), Cook Black Silicone (Cook Medical, Bloomington, IN, USA), Cook Universa Hydrogel (Cook Medical, Bloomington, IN, USA), Bard InLay (Bard Medical, Covington, GA, USA), and 2-hydroxyethyl methacrylate (HEMA)-coated Pellethane. HEMA-coated Pellethane was provided by Buddy D. Ratner, Ph.D., and his laboratory at the University of Washington (Seattle, WA, USA).[15,16] The HEMA-coating process is consistent with the previous report.[12] Cook Universa Hydrogel stent was used as the control material for experiments to maintain consistency with the previously reported study.[12] Based on the upper limit of SEM micrographs, all stent materials were manually cut into 8 mm length sections and weighed before the encrustation study.

2.2. Artificial Urine Solution. This study used two distinctive artificial urine conditions−−calcium phosphate-/struvite-forming and calcium oxalate-forming—to evaluate the stent materials resisting encrustation under different mineral composite-saturated solutions. The calcium phosphate/struvite AUS condition used here was a modified formula by Cox et al.[14] The calcium oxalate AUS condition is similar to that used by Malpass et al.[17] Table 1 lists the compositions of the AUS components used in this study. All chemicals, otherwise mentioned, were obtained from Millipore Sigma-Aldrich (Burlington, MA, USA). All solutions were independently prepared and combined using a peristaltic pump system in the reaction vessel. The initial pH of the calcium phosphate/struvite AUS was 5.5 upon mixing solutions A and B. The calcium phosphate/struvite AUS contained the enzyme urease, which converted urea to ammonium and carbon dioxide, such that the pH gradually increased and eventually stabilized at 8.5.[14,18] The calcium oxalate AUS maintained a pH of 6 upon mixing solutions A and B.[17] The two AUSs used in this study do not fully represent the mechanism of naturally occurring encrustations, mainly due to lacking a biofilm-forming element(s).

Table 1. Composition of Solutions A and B for Both Artificial Urine Solutions

calcium phosphate/struvite-forming AUS		calcium oxalate-forming AUS	
chemicals	conc. (mM)	chemicals	conc. (mM)
solution A (800 mL)		solution A (800 mL)	
potassium dihydrogen phosphate	56.00	sodium chloride	211.0
magnesium chloride hexahydrate	17.90	sodium dihydrogen phosphate	6.460
urea	266.4	magnesium sulfate	7.700
		calcium chloride dihydrate	8.000
		sodium citrate	6.400
solution B (800 mL)[a]		solution B (800 mL)	
calcium chloride dihydrate	24.28	sodium sulfate	33.90
chicken ovalbumin	0.470	potassium chloride	127.4
urease	2.600E−03	sodium oxalate	0.600
		sodium nitrate	2.000

[a]The solution is made fresh every 48 h due to the presence of proteins.

2.3. In Vitro Analysis of Stent Encrustation. Glass reaction vessels (Figure 1) with tightly fitted plastic lids were used for the batch−flow encrustation model. Every 24 h, 50% (200 mL) of AUSs would be removed from the reaction vessels and replaced with 100 mL of fresh solution from each solution A and B to mitigate the change in composition or premature depletion of salts in the AUS.[19−23] The peristaltic pump system was programmed to perform solution exchange daily at a precise time. Samples of the stents being investigated were suspended in the AUS through perforations in the lid using stiff PVC-coated wires. The experimental and AUS components were kept in an incubator at 37.0 °C ± 0.1 °C. Stent materials were removed at suitable time intervals and gently rinsed in distilled water, followed by air drying for 24 h at room temperature under a sterile fume hood prior to follow-up analysis.

2.4. Quantitative Analysis of Encrusted Materials on Stents. All experimental containers were prewashed with 1% nitric acid (Fisher Scientific, Hampton, NH) before ultra-trace elemental analysis via inductively coupled plasma mass spectrometry (ICP-MS). 11 week dried, encrusted stent specimens were submerged in 1 mL of 1% HNO_3 (v/v), followed by ultrasonication for 1 h using a Branson ultrasonic cleaner (Branson Ultrasonics Corp., Danbury, CT) to agitate, extract, and dissolve the encrusted minerals on the stents. Each sonicated sample was further diluted 100-fold in 1% HNO_3 to achieve a total dissolved solid of <1 weight percent (wt %) and a final volume of 10 mL before ICP-MS analysis. The presence of magnesium (Mg), calcium (Ca), and phosphorus (P) was measured by using an iCAP RQ inductively coupled plasma mass spectrometer with a Teledyne laser ablation (LA) system (Thermo Scientific, Waltham, MA, USA). Standard solutions of Mg, Ca, and P (Inorganic Ventures, Christiansburg, VA, USA) were used to generate a standard curve (100, 50, 20, and 0 ppm). One-way ANOVA was performed using GraphPad

https://doi.org/10.1021/acsomega.3c01800
ACS Omega 2023, 8, 29003−29011

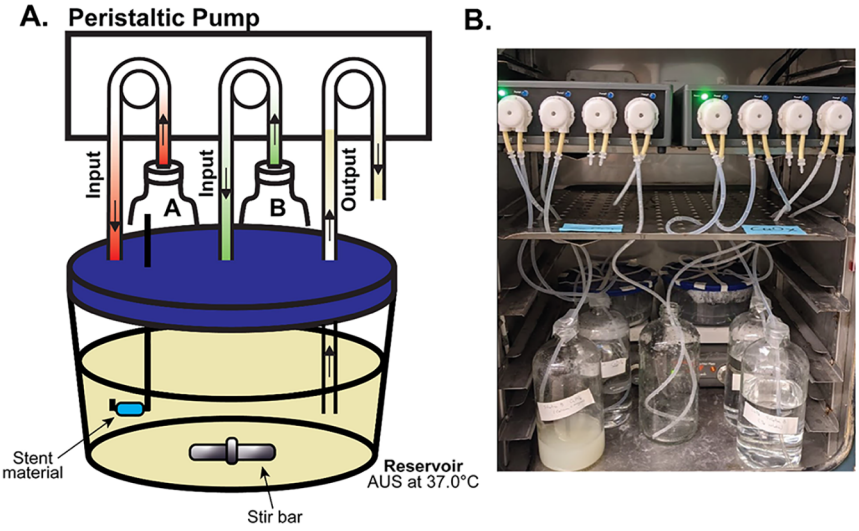

Figure 1. Peristaltic pump setup. (A) Reaction vessel setup for batch−flow encrustation model. The reaction vessel consists of a glass container with a tight-fit plastic lid. The lid is modified to include ports allowing solution exchange every 24 h. There are three ports, two input ports for pumping in fresh solutions of A and B to make the final artificial urine solution (AUS) and an output port for the removal of existing AUS. Samples are suspended in the AUS through perforations in the lid. The reaction vessel is kept in an incubator at 37.0 °C. The solution is constantly agitated with a magnetic stir bar at 300 RPM. (B) Final setup of the batch−flow experiment. The left is the calcium phosphate/struvite AUS apparatus, and the right is the calcium oxalate AUS apparatus.

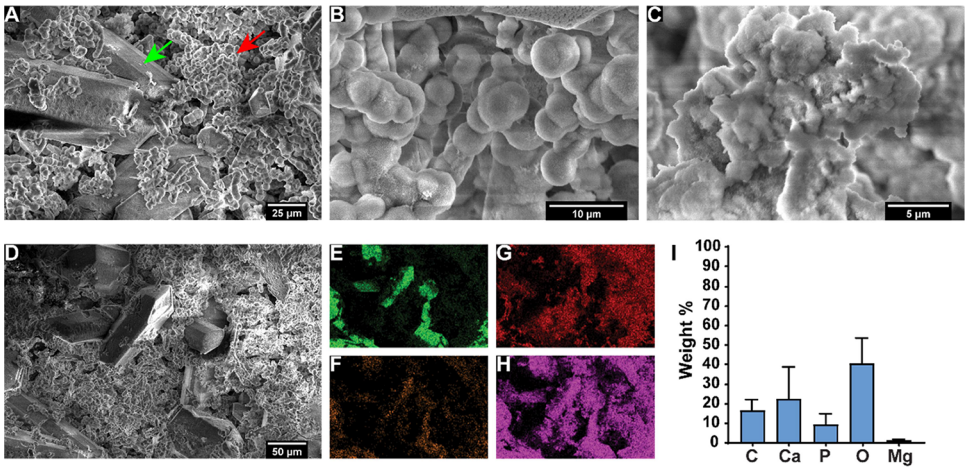

Figure 2. SEM and EDS analyses of encrusted crystals in different artificial urine solutions (AUSs). (A) Mixture of hydroxyapatite spheroid-like structured (red arrow) crystals and struvite (green arrow) crystals under the calcium phosphate/struvite AUS. (B) Close-up of the hydroxyapatite spheroid-like structured crystals observed in the calcium phosphate/struvite AUS. (C) Close-up of the crystals formed under the calcium oxalate AUS. (D) SEM and EDS of crystal deposits on the encrusted stent, and the following are the elemental breakdowns based on (E) magnesium, (F) nitrogen, (G) calcium, and (H) phosphorus. (I) Weight percent of elements encrusted on stents incubated in the calcium oxalate artificial urine. The dominant elements detected from the EDS analysis are oxygen (O), calcium (Ca), and carbon (C), indicating the formation of calcium oxalate. Additionally, the low amount of phosphorus (P) detected suggests that calcium oxalate is the preferred crystal that forms in the calcium oxalate AUS.

Prism (Dotmatics, Boston, MA, USA) to compare the amount of encrusted deposit on each stent material.

2.5. Surface Characterization of Encrusted Stents. SEM micrographs were acquired using a FEI Magellan 400 XHR system. EDS images were obtained using the same SEM system with an EDS detector (Oxford Instruments, 80 mm^2, with Aztec software). Before imaging, the samples were sputter-coated with ∼5 nm of iridium using a Q150T Plus turbomolecular pumped coater (Electron Microscopy Sciences, Hatfield, PA, USA). Accelerating voltages of incident electron beams ranged from 5 to 10 kV, and probe currents ranged from 0.4 to 1.6 nA. All SEM specimens were mounted on stainless steel stubs (Ted Pella, Redding, CA, USA) and held by carbon tapes (Ted Pella, Redding, CA, USA).

3. RESULTS

Two specific AUS conditions were used in the study to simulate the common stones that form in the urinary tract, such as metabolic stones (calcium oxalate) and infectious stones (struvite).[24,25] SEM was used to examine if distinct crystal structures formed under the different AUS conditions. Figure 2 shows that three specific crystal structures were observed. Both hydroxyapatite and struvite crystals were observed in the calcium phosphate/struvite AUS condition

https://doi.org/10.1021/acsomega.3c01800
ACS Omega 2023, 8, 29003−29011

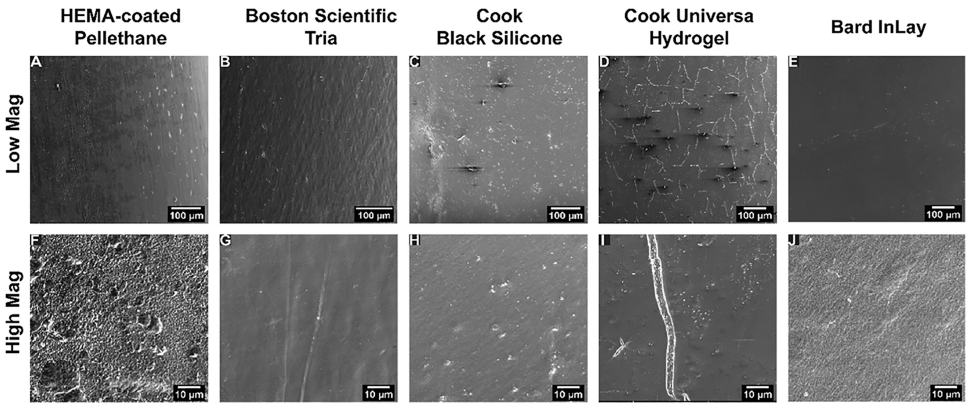

Figure 3. Scanning electron micrographs of the stents studied in this work. (A–E) Low-magnification images of the stents provide an overview of the surface. (F–J) Higher magnification images of the corresponding stents reveal features and textures on the surface, a possible reason for greater encrustation in the studied AUS environments.

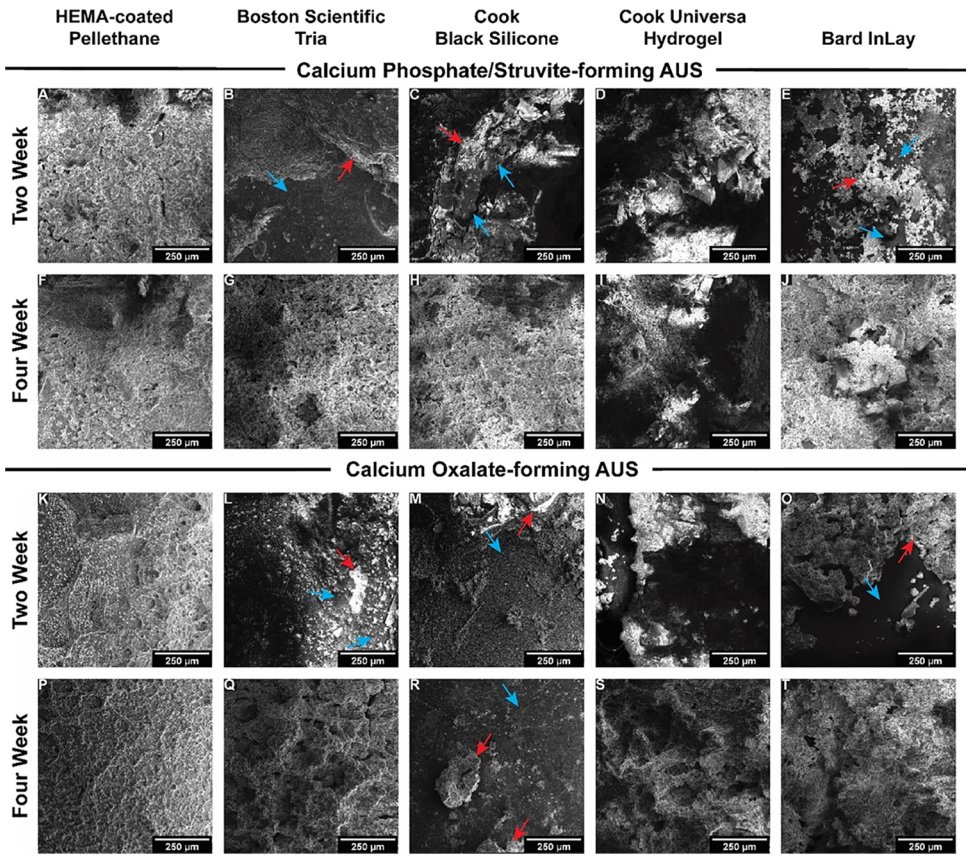

Figure 4. Scanning electron micrographs of encrusted stents after 2 and 4 weeks of incubation in calcium phosphate/struvite and calcium oxalate-forming AUS. SEM images of stents incubated in calcium phosphate-/struvite-forming artificial urine (A–J) and calcium oxalate-forming artificial urine (K–T). The blue arrows indicate the pristine stent surfaces, while the red arrows illustrate the encrusted areas. In both AUSs, at the 2 week time point, all stents showed some amount of encrustation, with the HEMA-coated Pellethane stent showing the most. At the 4 week time point, all stents in both AUSs, except for Cook Black Silicone (R), showed a great amount of encrustation. The Cook Black Silicone surface is highly visible with minimum encrustation, as indicated by the red arrows. We note that in (M, O), the dark regions are the pristine stent surface, while in (4D, I, N), the dark regions and lighter regions are due to a large amount of encrustation, leading to a dramatic height difference.

(Figure 2A,B), while calcium oxalate crystals were observed in the calcium oxalate AUS (Figure 2C).

EDS analysis was employed to identify the crystal compositions further. Figure 2D–H shows the EDS maps of two unique crystal formations in the calcium phosphate/struvite AUS based on the elemental compositions. The elemental map of magnesium, nitrogen, and phosphorus atoms (Figure 2E,F,H) distinctively highlighted the struvite crystals. Furthermore, the corresponding calcium atom elemental map (Figure 2G) showed no signal where the sites contain concentrated magnesium atoms, which suggested the formation of struvite crystals. Phosphorus was observed to dominate the EDS map (Figure 2H), which was expected since both hydroxyapatite and struvite crystals contain phosphate ions. Calcium ions were observed where the bulbiform crystals were located, indicating the hydroxyapatite crystals.

https://doi.org/10.1021/acsomega.3c01800
ACS Omega 2023, 8, 29003–29011

Table 2. Average Mass (mg) Changes of all Stent Samples after 11 Weeks' Incubation in Artificial Urine Conditions

	calcium phosphate/struvite			calcium oxalate		
stents	avg. initial weight (mg)	avg. final weight (mg)	avg. percent change in mass (%)	avg. initial weight (mg)	avg. final weight (mg)	avg. percent change in mass (%)
HEMA-coated Pellethane	24.6 ± 1.3	41.1 ± 2.7	66.9	23.8 ± 1.4	68.9 ± 6.7	189.8
Boston Scientific Tria	22.5 ± 0.8	31.0 ± 1.6	37.6	23.1 ± 0.3	30.0 ± 1.5	30.0
Cook Black Silicone	27.5 ± 0.6	26.0 ± 0.9	−5.3	28.5 ± 1.0	33.4 ± 0.9	17.2
Cook Universa Hydrogel	26.8 ± 0.9	39.9 ± 2.8	49.1	25.7 ± 1.6	55.4 ± 6.1	115.3
Bard InLay	25.2 ± 1.0	37.6 ± 1.6	49.1	22.5 ± 0.5	34.9 ± 5.0	55.2

Table 3. Average Mass (mg ± SD) of Elements Detected Encrusted on Stents after 11 Weeks of Incubation in Artificial Urine Solutions Using ICP-MS

	calcium phosphate/struvite			calcium oxalate		
stents	magnesium	phosphorus	calcium	magnesium	phosphorus	calcium
HEMA-coated Pellethane	0.215 ± 0.030	1.983 ± 0.169	3.853 ± 0.253	0.354 ± 0.038	5.516 ± 0.657	11.459 ± 1.313
Boston Scientific Tria	0.126 ± 0.027	0.991 ± 0.130	1.846 ± 0.243	0.077 ± 0.011	0.930 ± 0.179	1.861 ± 0.368
Cook Black Silicone	0.032 ± 0.007	0.226 ± 0.088	0.398 ± 0.187	0.056 ± 0.014	0.668 ± 0.187	1.332 ± 0.390
Cook Universa Hydrogel	0.180 ± 0.037	1.687 ± 0.263	3.272 ± 0.532	0.226 ± 0.011	3.247 ± 0.037	6.727 ± 0.148
Brad InLay	0.178 ± 0.023	1.626 ± 0.228	3.129 ± 0.438	0.109 ± 0.037	1.548 ± 0.608	3.111 ± 1.226

EDS was also used to confirm the formation of calcium oxalate crystals in the calcium oxalate AUS. As shown in Figure 2I, the percentage weight was calculated to show that carbon, calcium, and oxygen take up the highest percentage weight, indicating the presence of calcium oxalate. Moreover, phosphorus is observed in a lower weight percent composition. This is similar to previous literature reporting of EDS for calcium oxalate AUS.[26] However, the phosphorus weight percent is slightly higher than that previously reported, indicating that the AUS in this study might have formed a mixture of calcium oxalate and calcium phosphate.

3.1. SEM of Pristine Stents. SEM was used to assess the surfaces of each stent being investigated, as shown in Figure 3. The pristine HEMA-coated Pellethane stents exhibited the least smooth surface among the studied stents; high-magnification SEM images revealed a uniform but undulating and uneven surface generated by the chemical coating (Figure 3F). In addition, high-magnification images of the pristine Bard InLay stent revealed some minor ridged surface features and a diagonal striation pattern (Figure 3J). However, the Bard InLay surface appeared qualitatively smoother than the HEMA-coated Pellethane stent. SEM images showed that the Cook Universa Hydrogel stent contained wire-like structures, which appeared to be cracks in the outer layer when examined under a high magnification (Figure 3I). Lastly, SEM images showed the pristine Boston Scientific Tria and Cook Black Silicone as the smoothest surfaces with minimal surface features among the five stents (Figures 3G,H).

3.2. SEM of Encrusted Stents. SEM was used to qualitatively evaluate the rate of encrustation after 2 and 4 weeks of continuous incubation under the AUS conditions (Figure 4). The SEM analysis of stents that underwent continuous incubation of the calcium phosphate/struvite AUS after 2 weeks showed the complete encrustation of HEMA-coated Pellethane and Cook Universa Hydrogel (Figure 4A,D), while partial encrustation of Boston Scientific Tria, Cook Black Silicone, and Bard InLay, as shown in Figures 4B,C,E. After 4 weeks of continuous incubation, all stent materials were observed to be fully encrusted, as shown in Figure 4F−J. The deposited material from this AUS appeared to be amorphous with occasional distinct crystals.

The SEM analysis of stents subjected to continuous incubation of the calcium oxalate AUS after 2 weeks showed complete encrustation of the HEMA-coated Pellethane and Cook Universa Hydrogel stents, with no pristine surface visible (Figure 4K,N). In contrast, the Boston Scientific and Bard InLay stents showed partial encrustation as patches of native stent surface were still visible, as shown in Figures 4L,O. Cook Black Silicone showed the least encrustation among these stents (Figure 4M). SEM of the 4 week incubation showed all stents fully encrusted except for the Cook Black Silicone stent. The Cook Black Silicone stent remained relatively resistant to encrustation, even after 4 weeks of incubation in calcium oxalate AUS. The stent's original surface was still visible, as demonstrated in Figure 4R.

3.3. Stent Encrustation in Artificial Urine Conditions. The stent materials were assessed for their rate of encrustation throughout 11 weeks by measuring the eweight gain due to encrustation (Figure S1). The samples were carefully handled under sterile conditions to ensure minimum contamination risk. Each stent material was also evaluated in triplicates. In both AUS conditions, Cook Black Silicone stents had the least encrustation weight gain compared to the other four stents, while HEMA-coated Pellethane gained the most weight from encrustation, as illustrated in Table 2. The data also suggest that Boston Scientific Tria performed better than the Cook Universa Hydrogel and Bard InLay stents in resisting encrustation over 11 weeks. Finally, Cook Universa Hydrogel accumulated significant encrustation, as indicated by the weight gain, and the average percent change in mass is similar to that previously observed, demonstrating consistency between studies.[12] Lastly, Cook Black Silicone also showed a weight loss over the 11 weeks under the calcium phosphate-/struvite-forming AUS (Table 2). Further evaluation suggests that urease plays a role in the weight loss observed in the Black Silicone stents under the AUS (Figure S2).

3.4. ICP-MS Analysis of the Encrusted Stents. ICP-MS was used to quantify the major ionic components of the encrusted crystals (magnesium, calcium, and phosphorus)

https://doi.org/10.1021/acsomega.3c01800
ACS Omega 2023, 8, 29003−29011

deposited on the stent materials. All stent materials were observed to develop some encrustation; however, some had less encrustation than others, as illustrated by Table 3. Calcium was the most abundant material detected on the stents, while magnesium was the least abundant. HEMA-coated Pellethane was observed to have the highest amount of calcium deposited on its surface among the five stents, while Cook Black Silicone had the least. Boston Scientific Tria also had a relatively low amount of calcium and magnesium deposits detected on its surface. The ICP-MS data further reinforce the weight data (Figure S1) by showing a similar weight gain trend from the total Ca, Mg, and P deposits detected on each stent surface (Figure 5). Figure 5 also indicates the presence of encrustation

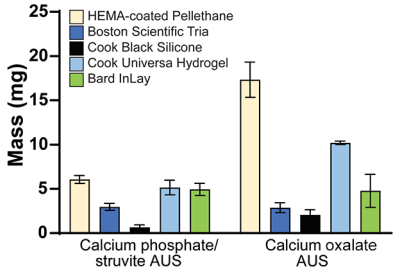

Figure 5. Total accumulated weight from Ca, Mg, and P based on ICP-MS analysis of the encrusted stents. The data show that HEMA-coated Pellethane accumulated the most deposits among the four other stents, while Cook Black Silicone and Boston Scientific Tria had the lowest deposits detected on their surfaces after 11 weeks of incubation in AUS. Experiments were done in triplicates; error bar = mean ± SD.

on Black Silicone stents, even though Table 2 displays that it lost weight. Furthermore, one-way ANOVA was performed to compare the amount of encrusted deposits on each stent material, as shown in Table 4.

4. DISCUSSION

To evaluate the encrustation resistance of stent materials, we established an automated batch−flow system in combination with two artificial urine conditions. SEM and EDS were used to confirm the crystals of the two different artificial urine models, as illustrated in Figure 2.

This study compared HEMA-coated Pellethane to four other commercially available stent materials to evaluate the best material for resisting encrustation under lithogenic artificial urine conditions. Previous research showed that HEMA-coated Pellethane resisted encrustation after 90 days of incubation in a lithogenic artificial urine environment, suggesting a promising biomaterial for urological stents.[12] Of note, the current results are contrary to that of the initial report. This is possibly due to the methodological differences that were used between the two studies. After qualitatively examining the HEMA-coated Pellethane stent under SEM after 2 weeks, the surface of the stent appeared to have a considerable amount of encrustation due to the presence of dense, web-like depositions. After 4 weeks, the SEM image for the HEMA-coated Pellethane stent showed an even greater density of the web-like depositions. The pristine stent surface was not visible at either of these two time points, which indicated robust encrustation within the first 2 weeks of indwell time. The surface readily accumulated deposits due to the uneven surface textures generated by the chemical coating,

Table 4. One-Way ANOVA Analysis Comparing the Accumulated Magnesium, Phosphorus, and Calcium Deposits Detected on Various Stent Materials by ICP-MS[aa]

stents		mean diff.	95% CI of diff.	*P*-value
Calcium Oxalate AUS				
HEMA-coated Pellethane	Boston Scientific Tria	14.46	11.84 to 17.08	<0.0001
	Cook Black Silicone	15.27	12.65 to 17.89	<0.0001
	Cook Universa Hydrogel	7.128	4.509 to 9.748	<0.0001
	Bard InLay	7.128	4.509 to 9.748	<0.0001
Boston Scientific Tria	Cook Black Silicone	0.8120	−1.807 to 3.431	n.s.
	Cook Universa Hydrogel	−7.333	−9.952 to −4.713	<0.0001
	Bard InLay	−7.333	−9.952 to −4.713	<0.0001
Cook Black Silicone	Cook Universa Hydrogel	−8.145	−10.76 to −5.525	<0.0001
	Bard InLay	−8.145	−10.76 to −5.525	<0.0001
Cook Universa Hydrogel	Bard InLay	0.000	−2.619 to 2.619	n.s.
Calcium Phosphate/Struvite AUS				
HEMA-coated Pellethane	Boston Scientific Tria	3.088	1.569 to 4.607	0.0004
	Cook Black Silicone	5.395	3.876 to 6.914	<0.0001
	Cook Universa Hydrogel	0.9110	−0.6079 to 2.430	n.s.
	Bard InLay	1.117	−0.4023 to 2.636	n.s.
Boston Scientific Tria	Cook Black Silicone	2.307	0.7877 to 3.826	0.0038
	Cook Universa Hydrogel	−2.177	−3.696 to −0.6581	0.0057
	Bard InLay	−1.971	−3.490 to −0.4524	0.0111
Cook Black Silicone	Cook Universa Hydrogel	−4.484	−6.003 to −2.965	<0.0001
	Bard InLay	−4.278	−5.797 to −2.759	<0.0001
Cook Universa Hydrogel	Bard InLay	0.2057	−1.313 to 1.725	n.s.

[a]n.s. = not significant.

leading to the increased surface area that allowed greater sites for crystal nucleation. In addition to this qualitative analysis, the weight data over 11 weeks showed that HEMA-coated Pellethane had the highest average mass gain under both lithogenic AUS conditions: an average of 66.9 and 189.8% weight gain from the encrusted deposit after 11 weeks of incubation in the calcium oxalate AUS and calcium phosphate/struvite AUS, respectively. Furthermore, ICP-MS analysis of the encrusted content showed that HEMA-coated Pellethane accumulated the most materials in both AUS conditions compared to the other stents, with calcium being the highest encrusted deposit. This suggests that the HEMA coating might be prone to accumulating calcium ions. This finding was corroborated in earlier biomaterials studies that used HEMA-based polymers.[27−29] For example, hydrogels of HEMA and methacrylic acid copolymers were found to accumulate a considerable amount of calcium ions when exposed to an aqueous solution with calcium.[29] Considering its natural affinity for calcium ions and the uneven chemical-coated

https://doi.org/10.1021/acsomega.3c01800
ACS Omega 2023, 8, 29003−29011

surface for possible element deposition and nucleation, HEMA-coated Pellethane would not be a suitable stent material.

In this study, the best-performing stent material was observed to be Cook Black Silicone, as it had the least amount of encrusted deposit buildup demonstrated under both experimental conditions, as shown in Tables 2 and 3. The pristine SEM images of Cook Black Silicone showed a relatively smoother surface compared to the other stents being investigated, especially compared to the HEMA-coated Pellethane. Furthermore, over the course of 2 weeks in both AUSs, the pristine surface of Cook Black Silicone remained visible, and only after 4 weeks of incubation in the calcium phosphate/struvite AUS was the stent completely encrusted. Moreover, the weight data over 11 weeks showed that Black Silicone had a minimum weight gain in both AUSs, with an average of −5.30% weight change in the calcium phosphate/struvite AUS and an average of 17.2% weight gain in the calcium oxalate AUS. Although the weight data showed a negative percentage in one of the AUS conditions, encrusted deposits were detectable through ICP-MS. The weight loss could be due to the enzyme urease degrading the surface coating of the Black Silicone stent (Figure S2). Urease had been previously documented to degrade polymers, such as polyurethane.[30,31] Unfortunately, the composition of the stent materials is proprietary; thus, the exact determination of weight loss was beyond the scope of the current study.

Based on the one-way ANOVA analysis (Table 4), the HEMA-coated Pellethane stent was found to have accumulated the most deposits under the calcium oxalate AUS compared to all other stent materials. However, Cook Universa Hydrogel and Bard InLay performed equally well as compared to each other in the calcium oxalate AUS but had more accumulated deposits compared to Black Silicone and Boston Scientific Tria. Black Silicone and Boston Scientific Tria stents were found to have the least mineral deposits and are comparable to each other. In the calcium phosphate/struvite AUS, HEMA-coated Pellethane, Cook Universa Hydrogel, and Bard InLay were found to have an equivalent amount of mineral deposits compared to Boston Scientific Tria and Black Silicone. Between Boston Scientific Tria and Black Silicone, Black Silicone stents were found to have the least mineral deposits in the calcium phosphate/struvite AUS.

The high resistance to encrustation deposit on Cook Black Silicone has been noted in several earlier studies.[18,32,33] For example, Tunney et al. showed that silicone was the least prone to encrustation after 14 weeks of incubation in lithogenic artificial urine, having 69% of its surface covered compared to 100% surface encrusted for all other stent materials tested.[33] It has been suggested that silicone is less prone to encrustation, most likely due to its smooth and nonsticky surface that reduces friction and absorption.[34,35] In our study, we purposely used urine prone to either calcium phosphate/struvite or calcium oxalate stone formation; in both instances, Cook Black Silicone had the least encrustation.

SEM of the pristine Boston Scientific Tria showed a smooth surface, while Bard InLay exhibited a rougher surface. Both Boston Scientific Tria and Bard InLay showed partial encrustation after 2 weeks in both AUS, similar to Cook Black Silicone. This is illustrated in Figure 4, where the pristine surfaces of both Boston Scientific Tria and Bard InLay were visible. However, both stents were fully encrusted after 4 weeks of incubation in both AUS conditions. In contrast, Cook Universa Hydrogel, like HEMA-coated Pellethane, was fully encrusted after 2 weeks of incubation in both AUS conditions. The uneven surface of Cook Universa Hydrogel, as shown in Figure 3, denoted by the wire-like characteristics, could have contributed to rapid encrustation. From the weight data (Table 2), it is observed that Boston Scientific Tria accumulated less encrusted mass than both Bard InLay and Cook Universa Hydrogel stents. Furthermore, the ICP-MS data showed that Boston Scientific Tria accumulated a relatively low amount of calcium, magnesium, and phosphorus after 11 weeks in the AUS conditions.

The current in vitro study demonstrated a higher amount of encrustation under the metabolic AUS condition compared to the infectious AUS condition, contrary to clinical observations.[36] These discrepancies can be attributed to the inherent limitations of an in vitro experimental setup. More specifically, struvite stones are a direct result of urease-forming bacteria (i.e., Proteus, Klebsiella, and Pseudomonas) and their ability to cultivate an alkaline environment that results in the formation of ammonium magnesium phosphate crystalline structures and matrices. Understandably, the matrices of mineral deposits, in combination with an increasing pH, result in a snowball effect in which they serve as a nidus for further bacterial colonization. Hence, an exponential rate of encrustation is seen, a feature not observed in an in vitro setting where the rate of encrustation is solely dependent on the concentration of minerals and urine flow rate.[37] Moreover, it is also important to note that non-struvite stone-formers are more likely to have metabolic derangements promoting their stone growth. However, the spectral nature of these derangements alongside the varying diets and urinary outflow rates among populations signifies how dynamic these stone-forming environments can be, with the stone growth varying from not at all to fully obstructing within months.[36] In comparison, our in vitro model provided a steady flow of urine that perpetually submerged all stents throughout an 11 week period and, thus, offered a higher, constant rate of encrustation that is likely not seen on average in an in vivo setting.

5. CONCLUSIONS

In this encrustation study, using two types of lithogenic artificial urine, HEMA-coated Pellethane performed worse than all other ureteral stent materials tested. The combination of rough surfaces generated by the HEMA coating and HEMA's affinity for calcium promoted excessive encrustation. Of the stent materials tested, Cook Black Silicone showed the greatest resistance to encrustation with the smallest weight gain and the longest indwelling time without significant surface encrustation.

There are many aspects to consider in ureteral stent design in minimizing encrustation. One common strategy in reducing encrustation is developing novel chemical coatings for stent surfaces that exhibit inhibition and resistance to the nucleation of deposited elements and bacterial adhesion.[5] For example, hydrogels have been explored as the possible chemical coatings for ureteral stents in this regard.[33,38,39] More recently, bioinspired stent coatings, such as chondroitin sulfate, have been analyzed to address the perpetual problem of stent encrustation.[40,41]

In addition to exploring novel chemical coatings for ureteral stents, understanding the chemical properties of the material surface is also essential in reducing encrustation. Rebl et al. recently studied the surface chemical features, such as the

https://doi.org/10.1021/acsomega.3c01800
ACS Omega 2023, 8, 29003−29011

contact angle and surface charge, to better understand the surface characteristics that play a role in encrustation formation.[42] The published finding suggests that material surfaces that are slightly hydrophobic with a strong negative zeta potential helped limit the deposition of crystals and resisted biofilm formation.[42] Additionally, studies that characterize and evaluate the surface chemistry of commercially available stents and their propensity to encrust can provide clinical value. The analysis of commercially available stents through techniques such as contact-angle measurements, FTIR (Fourier transform infrared)/Raman spectroscopy, and XPS can provide additional unique insights into the mechanisms of encrustation. However, investigating commercially available stents can prove challenging due to their cylindrical geometry in nature. Therefore, all these surface characteristics and features will need to be carefully considered when designing future ureteral stents to minimize encrustation.

■ ASSOCIATED CONTENT

Supporting Information

The Supporting Information is available free of charge at https://pubs.acs.org/doi/10.1021/acsomega.3c01800.

Additional experimental details, materials, and methods, such as the encrustation weight data over 11 weeks of incubation in artificial urine; urease activity; urease degradation of stent materials; and atomic force microscopy (PDF)

■ AUTHOR INFORMATION

Corresponding Author

Yi X. Wu − *Department of Urology, University of California, Irvine, Orange 92868 California, United States;* orcid.org/0000-0001-7833-1481; Phone: +1 (901) 216-4582; Email: yxwu@hs.uci.edu; Fax: +1-888-3378-4358

Authors

Eric J. Choi − *Department of Chemistry, University of California, Irvine, Irvine 92697 California, United States;* orcid.org/0000-0003-3287-1284

Amberly A. Vu − *Department of Urology, University of California, Irvine, Orange 92868 California, United States*

Pengbo Jiang − *Department of Urology, University of California, Irvine, Orange 92868 California, United States*

Sohrab N. Ali − *Department of Urology, University of California, Irvine, Orange 92868 California, United States*

Roshan M. Patel − *Department of Urology, University of California, Irvine, Orange 92868 California, United States*

Jaime Landman − *Department of Urology, University of California, Irvine, Orange 92868 California, United States*

Ralph V. Clayman − *Department of Urology, University of California, Irvine, Orange 92868 California, United States*

Complete contact information is available at: https://pubs.acs.org/10.1021/acsomega.3c01800

Author Contributions

Conceptualization: Y.X.W. and R.V.C.; methodology: Y.X.W., E.J.C., and A.A.V.; validation: Y.X.W., E.J.C., and A.A.V.; formal analysis: Y.X.W., E.J.C., and A.A.V.; investigation: Y.X.W., E.J.C., and A.A.V.; data curation: Y.X.W., E.J.C., and A.A.V.; writing−−original draft: Y.X.W., E.J.C., S.N.A., and R.V.C.; writing−−review and editing: Y.X.W., E.J.C., S.N.A., P.J., R.M.P., J.L., and R.V.C.; visualization: Y.X.W. and E.J.C.; supervision: Y.X.W., R.M.P., J.L., and R.V.C., project administration: Y.X.W., R.M.P., J.L., and R.V.C.; photo contribution: Y.X.W.

Funding

This research received no specific grant from any funding agency in the public, commercial, or not-for-profit sectors.

Notes

The authors declare no competing financial interest.

■ ACKNOWLEDGMENTS

SEM, EDS, and ICP-MS were carried out at the University of California, Irvine Materials Research Institute (IMRI). HEMA-coated Pellethane was provided by Buddy D. Ratner, Ph.D., and his laboratory at the University of Washington.

■ REFERENCES

(1) Assimos, D.; et al. Surgical Management of Stones: American Urological Association/Endourological Society Guideline, PART II. *J. Urol.* **2016**, *196*, 1161−1169.

(2) Smith, A.; et al. Optimizing Outcomes in Urological Surgery: Postoperative Care. *Urol. Pract.* **2020**, *7*, 521−529.

(3) Zimskind, P. D.; Fetter, T. R.; Wilkerson, J. L. Clinical use of long-term indwelling silicone rubber ureteral splints inserted cystoscopically. *J. Urol.* **1967**, *97*, 840−844.

(4) Arkusz, K.; Pasik, K.; Halinski, A.; Halinski, A. Surface analysis of ureteral stent before and after implantation in the bodies of child patients. *Urolithiasis* **2021**, *49*, 83−92.

(5) Tomer, N.; Garden, E.; Small, A.; Palese, M. Ureteral Stent Encrustation: Epidemiology, Pathophysiology, Management and Current Technology. *J. Urol.* **2021**, *205*, 68−77.

(6) Alsikafi, N. F.; et al. Prospective evaluation of ureteral stent durability in patients with chronic ureteral obstruction. *Urology* **2002**, *59*, 847−850.

(7) Fiuk, J.; Bao, Y.; Calleary, J. G.; Schwartz, B. F.; Denstedt, J. D. The use of internal stents in chronic ureteral obstruction. *J. Urol.* **2015**, *193*, 1092−1100.

(8) Lange, D.; Bidnur, S.; Hoag, N.; Chew, B. H. Ureteral stent-associated complications–where we are and where we are going. *Nat. Rev. Urol.* **2015**, *12*, 17−25.

(9) Miyaoka, R.; Monga, M. Ureteral stent discomfort: Etiology and management. *Indian J. Urol.* **2009**, *25*, 455−460.

(10) Osman, N. I.; Collins, G. N. Urological litigation in the UK National Health Service (NHS): an analysis of 14 years of successful claims. *BJU Int.* **2011**, *108*, 162−165.

(11) Sancaktutar, A. A.; Soylemez, H.; Bozkurt, Y.; Penbegul, N.; Atar, M. Treatment of forgotten ureteral stents: how much does it really cost? A cost-effectiveness study in 27 patients. *Urol. Res.* **2012**, *40*, 317−325.

(12) Cottone, C. M.; et al. Surface-Treated Pellethanes: Comparative Quantification of Encrustation in Artificial Urine Solution. *J. Endourol.* **2020**, *34*, 868−873.

(13) Marois, Y.; Guidoin, R. In *Madame Curie Bioscience Database [Internet]*; Landes Bioscience, 2013.

(14) Cox, A. J.; Hukins, D. W.; Davies, K. E.; Irlam, J. C.; Sutton, T. M. An automated technique for in vitro assessment of the susceptibility of urinary catheter materials to encrustation. *Eng. Med.* **1987**, *16*, 37−41.

(15) Lopez, G. P.; Ratner, B. D.; Rapoza, R. J.; Horbett, T. A. Plasma deposition of ultrathin films of poly (2-hydroxyethyl methacrylate): surface analysis and protein adsorption measurements. *Macromolecules* **1993**, *26*, 3247−3253.

(16) Ratner, B. D.; Chilkoti, A.; Lopez, G. P. *Plasma deposition, treatment and etching of polymers*, 1990; pp 463 −516.

(17) Malpass, C. A.; Millsap, K. W.; Sidhu, H.; Gower, L. B. Immobilization of an oxalate-degrading enzyme on silicone elastomer. *J. Biomed. Mater. Res.* **2002**, *63*, 822−829.

(18) Tunney, M. M.; Keane, P. F.; Gorman, S. P. Assessment of urinary tract biomaterial encrustation using a modified Robbins device continuous flow model. *J. Biomed. Mater. Res.* **1997**, *38*, 87−93.
(19) Desgrandchamps, F.; Moulinier, F.; Daudon, M.; Teillac, P.; Le Duc, A. An in vitro comparison of urease-induced encrustation of JJ stents in human urine. *Br. J. Urol.* **1997**, *79*, 24−27.
(20) Gorman, S. P.; Garvin, C. P.; Quigley, F.; Jones, D. S. Design and validation of a dynamic flow model simulating encrustation of biomaterials in the urinary tract. *J. Pharm. Pharmacol.* **2010**, *55*, 461−468.
(21) Tunney, M. M.; Bonner, M. C.; Keane, P. F.; Gorman, S. P. Development of a model for assessment of biomaterial encrustation in the upper urinary tract. *Biomaterials* **1996**, *17*, 1025−1029.
(22) Tunney, M. M.; Jones, D. S.; Gorman, S. P. Biofilm and biofilm-related encrustation of urinary tract devices. *Methods Enzymol.* **1999**, *310*, 558−566.
(23) Zhang, Y.; He, J.; Chen, H.; Xiong, C. A new hydrophilic biodegradable ureteral stent restrain encrustation both in vitro and in vivo. *J. Biomater. Appl.* **2021**, *35*, 720−731.
(24) Denstedt, J. D.; Wollin, T. A.; Reid, G. Biomaterials used in urology: current issues of biocompatibility, infection, and encrustation. *J. Endourol.* **1998**, *12*, 493−500.
(25) Griffith, D. P.; Musher, D. M.; Itin, C. Urease. The primary cause of infection-induced urinary stones. *Invest. Urol.* **1976**, *13*, 346−350.
(26) Shafat, M.; Rajakumar, K.; Syme, H.; Buchholz, N.; Knight, M. M. Stent encrustation in feline and human artificial urine: does the low molecular weight composition account for the difference? *Urolithiasis* **2013**, *41*, 481−486.
(27) Levy, B. Calcium deposits on glyceryl methyl methacrylate and hydroxyethyl methacrylate contact lenses. *Am. J. Optom. Physiol. Opt.* **1984**, *61*, 605−607.
(28) Montheard, J.-P.; Chatzopoulos, M.; Chappard, D. 2-Hydroxyethyl methacrylate (HEMA): chemical properties and applications in biomedical fields. *J. Macromol. Sci., Part C: Polym. Rev.* **1992**, *32*, 1−34.
(29) Van-De-Mark, M. R.; Lian, N. D.; Brandon, M.; Eckstein, E. C. *Interaction of calcium with HEMA/MAA copolymers*, 1987.
(30) Howard, G. T. Biodegradation of polyurethane: a review. *Int. Biodeterior. Biodegrad.* **2002**, *49*, 245−252.
(31) Phua, S. K.; Castillo, E.; Anderson, J. M.; Hiltner, A. Biodegradation of a polyurethane in vitro. *J. Biomed. Mater. Res.* **1987**, *21*, 231−246.
(32) Beiko, D. T.; Knudsen, B. E.; Denstedt, J. D. Advances in ureteral stent design. *J. Endourol.* **2003**, *17*, 195−199.
(33) Tunney, M. M.; Keane, P. F.; Jones, D. S.; Gorman, S. P. Comparative assessment of ureteral stent biomaterial encrustation. *Biomaterials* **1996**, *17*, 1541−1546.
(34) Gadzhiev, N.; et al. Comparison of silicone versus polyurethane ureteral stents: a prospective controlled study. *BMC Urol.* **2020**, *20*, 10.
(35) Bruce, A. W.; Sira, S. S.; Clark, A. F.; Awad, S. A. The problem of catheter encrustation. *Can. Med. Assoc. J.* **1974**, *111*, 238−239. passim
(36) Karki, N.; Leslie, S. W. Struvite And Triple Phosphate Renal Calculi. *StatPearls [Internet]* **2022**.
(37) Kram, W.; Buchholz, N.; Hakenberg, O. W. Ureteral stent encrustation. Pathophysiology. *Arch. Esp. Urol.* **2016**, *69*, 485−493.
(38) De Grazia, A.; Somani, B. K.; Soria, F.; Carugo, D.; Mosayyebi, A. Latest advancements in ureteral stent technology. *Transl. Androl. Urol.* **2019**, *8*, S436−S441.
(39) Gorman, S. P.; Tunney, M. M.; Keane, P. F.; Van Bladel, K.; Bley, B. Characterization and assessment of a novel poly(ethylene oxide)/polyurethane composite hydrogel (Aquavene) as a ureteral stent biomaterial. *J. Biomed. Mater. Res.* **1998**, *39*, 642−649.
(40) Yao, Q.; et al. Bio-inspired antibacterial coatings on urinary stents for encrustation prevention. *J. Mater. Chem. B* **2022**, *10*, 2584−2596.
(41) Yuan, H.; Qian, B.; Chen, H.; Lan, M. The influence of conditioning film on antifouling properties of the polyurethane film modified by chondroitin sulfate in urine. *Appl. Surf. Sci.* **2017**, *426*, 587−596.
(42) Rebl, H.; et al. Prevention of encrustation on ureteral stents: which surface parameters provide guidance for the development of novel stent materials? *Polymer* **2020**, *12*, 558.

https://doi.org/10.1021/acsomega.3c01800
ACS Omega 2023, 8, 29003−29011